

Energetic particle induced intra-seasonal-annual variability of ozone inside the Antarctic polar vortex observed in satellite data

T. Fytterer¹, M. G. Mlynczak², H. Nieder¹, K. Pérot³, M. Sinnhuber¹, G. Stiller¹, and J. Urban^{3†}

[1]{Institute for Meteorology and Climate Research, Karlsruhe Institute of Technology, Eggenstein-Leopoldshafen, Germany}

[2]{Atmospheric Sciences Division, NASA Langley Research Center, Hampton, VA}

[3]{Department of Earth and Space Sciences, Chalmers University of Technology, Göteborg, Sweden}

[†]J. Urban passed away on 14 August 2014

Correspondence to: T. Fytterer (tilo.fytterer@kit.edu)

Abstract

Measurements from 2002 – 2011 by three independent satellite instruments, namely MIPAS, SABER, and SMR on board the ENVISAT, TIMED, and Odin satellites are used to investigate the intra-seasonal-annual variability of stratospheric and mesospheric O₃ volume mixing ratio (vmr) inside the Antarctic polar vortex due to solar and geomagnetic activity. In this study, we individually analysed the relative O₃ vmr variations between maximum and minimum conditions of a number of solar and geomagnetic indices (F10.7 cm solar radio flux, Ap index, ≥ 2 MeV electron flux). The indices are 26-day averages centred at 1 April, 1 May, and 1 June while O₃ is based on 26-day running means from 1 April - 1 November at altitudes from 20 - 70 km. During solar quiet time from 2005 – 2010, the composite of all three instruments reveals an apparent negative O₃ signalfeedback associated to the geomagnetic activity (Ap index) around 1 April, on average reaching amplitudes between -5% and -10% of the respective O₃ background. The O₃ response exceeds the significance level of 95% and propagates downwards throughout the polar winter from the stratopause down to ~ 25 km. These observed results are in good qualitative agreement with the O₃ vmr pattern simulated with a three-dimensional chemistry-transport model, which includes

1 particle impact ionisation.

2

3 **1 Introduction**

4 Energetic particles (~keV - ~MeV), mainly originating from the sun but also from the Earth's
5 magnetospheric radiation belts and the aurora region, penetrate the atmosphere down to
6 mesospheric and stratospheric regions, depending on their energy. The particles are guided by the
7 Earth's magnetic field lines and therefore mostly precipitate at auroral and radiation belt areas (~55°
8 - 70° geomagnetic latitudes), depositing energy and directly influencing the chemical composition
9 of the stratosphere and mesosphere. Due to the air compounds, precipitating particles mainly
10 produce large abundances of O_2^+ as well as $N(^2D)$ and N_2^+ . $N(^2D)$ and N_2^+ lead to increased
11 concentrations of odd nitrogen ($NO_x = N + NO + NO_2$) through a number of reactions, including
12 dissociative recombination of N_2^+ and ion-neutral chemistry with species of the oxygen family (e.g.
13 Rusch et al., 1981). Additionally, O_2^+ and water vapour initialise chain reactions associated with
14 water cluster ion formation and accompanied recombination reactions, which eventually lead to the
15 production of odd hydrogen ($HO_x = H + OH + HO_2$; e.g. Solomon et al., 1981).

16 Both HO_x and NO_x play an important role in destroying O_3 in the mesosphere and stratosphere (e.g.
17 Lary, 1997). However, HO_x is short-lived (~seconds – hours) and therefore more important near its
18 source region in the mesosphere, while NO_x has a relatively long life time (~days - months), at least
19 during night-time conditions. Consequently, NO_x can be transported downwards inside the polar
20 vortex (e.g. Solomon et al., 1982) from the upper mesosphere/lower thermosphere down to the
21 stratosphere, resulting in stratospheric O_3 depletion through catalytic chemical reactions in
22 combination with solar radiation. Thus, energetic particle precipitation (EPP) indirectly affects O_3
23 during polar winter. Since O_3 is the major radiative heating source in the stratosphere, variations of
24 this gas will also influence the stratospheric temperature field and eventually lead to altered
25 atmospheric dynamics. However, the atmospheric response to EPP is not fully understood so far.
26 The current knowledge is discussed in more detail by Sinnhuber et al. (2012).

27 Observations of the EPP indirect effect on stratospheric polar O_3 are relatively rare, at least
28 compared to other latitudes, due to a lack of long-term O_3 measurements in these regions. However,
29 a hint for this mechanism was presented by Randall et al. (1998) which analysed the Polar Ozone
30 and Aerosol Measurement instrument data, revealing a close anticorrelation between NO_2 and O_3
31 mixing ratios in winter/spring from 1994 – 1996 in the Antarctic stratosphere (~25 – 35 km). They
32 suggested that the relationship cannot originate from downwards transported O_3 -deficient air but is

1 due to photochemical destruction of O_3 by NO_2 . Further observations from several satellite
2 instruments from 1992 – 2005 show that the stratospheric NO_x enhancement in the Southern
3 Hemisphere is caused by EPP (Randall et al., 2007). More recent satellite observations from 2002 –
4 2012 reported by Funke et al. (2014) reveal that particle induced NO_x is indeed transported
5 downwards to the middle stratosphere at polar latitudes, while further model studies suggest that the
6 subsiding of NO_x leads to strongly reduced stratospheric O_3 concentrations (~30%) down to
7 altitudes ~30 km (e.g. Reddmann et al., 2010). Thus, it appears promising to search for a link
8 between EPP and O_3 in actual data sets, because the downwards propagating signal of the EPP
9 indirect effect on stratospheric and mesospheric O_3 throughout the polar winter has not been
10 explicitly observed so far. Note that, NO_x can be only transported downwards inside a stable large-
11 scale dynamical structure, which provides sufficient subsidence and prevents NO_x removal/dilution
12 by horizontal transport. These conditions are found primarily inside the Antarctic polar vortex,
13 because the Arctic vortex is strongly disrupted by planetary waves, leading to its weakening or
14 temporary breakdown. This large dynamical variability eventually causes high variations in O_3
15 volume mixing ratios (vmr), superposing the EPP indirect effect.

16 Therefore our study is focused on O_3 vmr observations inside the Antarctic polar vortex from ~20 –
17 70 km, derived from ENVironmental SATellite/Michelson Interferometer for Passive Atmospheric
18 Sounding (ENVISAT/MIPAS), Thermosphere Ionosphere Mesosphere Energetics and
19 Dynamics/Sounding of the Atmosphere using Broadband Emission Radiometry (TIMED/SABER),
20 and Odin/Sub-Millimetre Radiometer (SMR) measurements. The ~~intra-seasonal~~ ~~annual~~ variability
21 of the O_3 vmr values has been investigated and the relation to a number of solar and geomagnetic
22 indices, namely the F10.7 cm solar radio flux, the Ap index, and the ≥ 2 MeV electron flux is
23 analysed.

24

25 **2 Data analysis and numerical modelling**

26 **2.1 Approximation of the Antarctic polar vortex**

27 The position and the extension of the Antarctic polar vortex were estimated by using the gradient of
28 the potential vorticity (PV) on isentropic surfaces (Nash et al., 1996). Assuming a dry atmosphere at
29 altitudes ≥ 20 km, the PV was calculated from temperature, pressure, relative vorticity, and the
30 corresponding latitude taken from ERA-Interim (<https://ecaccess.ecmwf.int/ecmwf>), the latest
31 version of global atmospheric reanalysis data produced by the European Centre for Medium-Range

1 Weather Forecasts (ECWMF). The reference pressure was set to 1000 hPa and the gravitational
2 constant was considered to be dependent on latitude and height. The PV was calculated for all
3 height intervals between 20 km and 70 km which were adapted from the MIPAS retrieval grid (see
4 Sect. 2.2.1). Note that ERA-Interim data is primarily model-driven at mesospheric altitudes but the
5 individual PV results look reasonable at each height interval. As an example, Fig. 1 shows the PV,
6 depending on time and equivalent latitude (EQL), during the Antarctic winter 2011 at ~40 km. The
7 EQLs assigned to an individual PV isoline enclose the same area as the geographical latitudes of
8 equivalent values. However, this area is located around an estimate of the vortex centre position,
9 rather than around the geographical pole. In general, the EQL of the strongest PV gradient indicates
10 the estimated location of the vortex edge, however, in most cases, there are at least two locations
11 revealing gradients of similar magnitude. Therefore, Nash et al. (1996) also considered the zonal
12 wind to locate the real vortex edge, but here we added a visual analysis instead of the zonal wind to
13 divide the Southern Hemisphere into three non-overlapping zones: deep inside the Antarctic polar
14 vortex (CORE) and the corresponding outermost edge (EDGE), covering all EQLs poleward the
15 respective borders, as well as an area not influenced by the vortex (OUTSIDE), which extends from
16 the equator to the respective OUTSIDE border. In this study we will consider the EDGE region as
17 the Antarctic vortex area, but the CORE and OUTSIDE region are still necessary to determine
18 whether the observed features inside the EDGE zone are actually originating from the vortex itself.
19 The limits of the three regions of each height interval revealed no strong variation from 2002 -
20 2011, therefore holding for every winter (Table 1). Note that the ECMWF ERA-Interim data only
21 covers heights up to ~63 km. However, considering the behaviour of the Antarctic vortex at
22 altitudes between 60 km and 70 km (Preusse et al., 2009, their Fig. 2a), it seems reasonable to
23 assume that the estimated limits of the three regions at ~63 km are also valid up to 70 km.

24 **2.2 Ozone measurements**

25 **2.2.1 MIPAS**

26 MIPAS (Fischer et al., 2008) was a limb sounder on board ENVISAT, which had a sun-synchronous
27 orbit. The main advantages of MIPAS measurements are the global coverage from 87°S – 89°N and
28 the availability of observations during both day and night, crossing the equator at ~10:00 LT and
29 ~22:00 LT, respectively. MIPAS was a Fourier transform infrared (4.15 μm - 14.6 μm) emission
30 spectrometer, allowing simultaneous observations of several atmospheric trace gases, including O₃.
31 MIPAS was operational from July 2002 – April 2012, but due to an instrumental failure in March

1 2004, the entire observation period is divided into two subintervals from July 2002 – March 2004
2 and January 2005 – April 2012 (referred to as P1 and P2 here, respectively). During P1 an almost
3 continuous time series is available, while larger data gaps are present during P2 before October
4 2006. Here, we use the complete data set of the most frequent observation mode (nominal mode),
5 covering the altitudes from the upper troposphere up to ~70 km at the poles which was derived from
6 the MIPAS level-2 research processor developed by IMK/IAA. Details of the retrievals are
7 described in von Clarmann et al. (2003), Glatthor et al. (2006), and von Clarmann et al. (2009).
8 Note that the number of tangent heights is constant during P1 (17) and P2 (23), and that the actually
9 available altitudes (cloud contaminated observations are disregarded) only slightly differ from day
10 to day. The corresponding vertical resolution becomes coarser at higher altitudes (independent of
11 the geographical location), increasing from 3.5 to 8 km (Steck et al., 2007) and from 2.5 to 5 km
12 (Eckert et al., 2014) in P1 and P2, respectively. However, the retrieval grid in all MIPAS O₃ data
13 versions used here (V3O_O3_9, V5R_O3_220, V5R_O3_221) is independent of the tangent
14 heights, with a grid width of 1 km below 44 km and 2 km above. During P1/P2 O₃ was measured at
15 two different wavelength intervals, ranging from 9.0 – 9.4 μm/9.6 – 9.7 μm and 12.5 – 13.5
16 μm/12.7 – 13.2 μm in particular. However, not the full spectral ranges were used, but sub-intervals
17 (microwindows). These were selected to minimise the computing time and to optimize the relation
18 between the measurement-noise induced random error and other errors. These other errors originate,
19 among further error sources, from spectral contributions of further atmospheric constituents of
20 unknown abundances. It should also be noted that there is a bias in MIPAS O₃ data between the two
21 periods, which was estimated using a multi-linear parametric trend model (Eckert et al., 2014). To
22 accept an O₃ data point, the recommended filter criteria for MIPAS O₃ data were applied by using
23 an averaging kernel diagonal value >0.03 as well as the visibility flag = 1 which indicates spectral
24 available data.

25 At least 10 accepted data points inside the Antarctic polar vortex at a certain grid level were
26 required to calculate the arithmetic average of one day, while at least 13 days were arithmetically
27 averaged to a 26-day running mean from 1 April – 1 November, repeating this algorithm for each
28 height interval and all years from 2002 - 2011. The time interval of 26 days was chosen to minimise
29 a possible influence of the 27-day cycle of the sun, also ensuring that each time interval includes
30 only one 27-day solar rotation maximum at most. The analysis was repeated for NO₂
31 (V5R_NO2_220, V5R_NO2_221) and the corresponding retrieval is described in Funke et al.
32 (2005) and Funke et al. (2011).

33 **2.2.2 SABER**

1 The SABER instrument on board the TIMED Satellite has been nearly continuously operating since
2 January 2002, measuring vertical profiles of several atmospheric parameters and minor constituents
3 (e.g. O₃) from the surface up to altitudes >100 km. The SABER measurements are governed by a
4 periodic quasi 60-day cycle, each time changing from the Southern Hemisphere mode (83°S –
5 52°N) to the Northern Hemisphere mode (52°S – 83°N) and vice versa. Note that the “switching
6 day” is only varying a few days from year to year. To consider both day and night O₃ observations,
7 SABER Level 2A Ozone96 data v2.0 and v1.07 (<http://saber.gats-inc.com/custom.php>, Rong et al.,
8 2009) measured at ~9.6 μm are used. However, v1.07 was only used to fill v2.0 data gaps, which
9 seemed reasonable because the data fit quite well the results of the performed analysis during the
10 respective periods (15 May – 31 May, 7 August – 31 August, not shown here). Consequently, the
11 combined data set of both versions shows no larger data gap and the measurements of both versions
12 were restricted to values <20 ppm to exclude outliers. Comparisons with the results of an increased
13 threshold to <100 ppm revealed only minor differences (not shown here). The investigated height
14 interval, ranging from 20 to 70 km, is divided in 38 non-overlapping subintervals and binned at the
15 same altitudes as MIPAS data. The algorithm used to calculate the running means is also identical to
16 the one applied for the “accepted” MIPAS data points. However, SABER needs approximately 60
17 days to cover all local times, leading to a quasi 60-day wave like oscillation in O₃ if 26-day running
18 means are used. This behaviour becomes evident at altitudes >50 km, where the averaging interval
19 was consequently extended from 26 to 60 days. Note that the calculation of the 60-day running
20 means required at least 30 days.

21 **2.2.3 SMR**

22 The Odin satellite mission started in February 2001 and is a joint project between Sweden, Canada,
23 France and Finland (Murtagh et al., 2002). Odin was launched into a sun-synchronous polar orbit,
24 carrying the SMR instrument and nominally covering the latitude range from 82.5°S – 82.5°N. The
25 SMR makes vertical profile measurements during both day and night, while passing the equator at
26 ~6:00/18:00 LT in the descending/ascending node. The O₃ data were extracted from the Odin/SMR
27 Level 2 data product, version 2.0 (<http://odin.rss.chalmers.se/>, Urban et al., 2005), only using
28 measurements of the frequency band centred around ~544.6 GHz, providing vertical O₃ profiles in
29 the ~15-70 km altitude range. The filtering criterion used for SMR is the measurement response,
30 which corresponds to the sum of the rows of the averaging kernel matrix. The profiles characterized
31 by a measurement response lower than 0.9 are not reliable enough, and are therefore excluded. The
32 algorithm to calculate the 26-day running means is identical to the one applied to MIPAS data. Note
33 that Odin/SMR was a two-discipline satellite until April 2007, switching between atmospheric

1 (aeronomy mode) and astronomy observations, and is entirely dedicated to aeronomy since this
2 date. Additionally, measurements in the relevant mode are only performed every day, consequently
3 only covering about one day out of three before April 2007 and every other day afterwards.
4 However, the calculation of the 26-day running means is still possible because the data gaps occur
5 in a regular way, so they do not essentially worsen the 26-day averages. The vertical resolution of
6 the data version used here is better than 3 km below 45 km, but increases to 5 – 6 km (50 – 60 km)
7 and 7 – 10 km (60 – 70 km), leading to noisy results at altitudes >50 km compared to the other two
8 instruments.

9 **2.3 Solar data and geomagnetic indices**

10 The data of the indices were obtained from two different websites provided by the National
11 Geophysical Data Center. In detail the flux of the 10.7 cm radio emission from the sun (F10.7) and
12 the geomagnetic Ap index (Ap), commonly used proxies for solar variation and geomagnetic
13 activity, respectively, were downloaded from <http://spidr.ngdc.noaa.gov/spidr/>. The ≥ 2 MeV
14 electron flux (2 MeV), including the flux of all electrons with energy levels above 2 MeV, was ~~used~~
15 ~~here as an indicator of the influence from the magnetosphere. The corresponding time series were~~
16 measured by the Geostationary Operational Environmental Satellites (GOES) and ~~the~~
17 ~~corresponding~~ time series were downloaded from
18 ftp://ftp.ngdc.noaa.gov/STP/SOLAR_DATA/SATELLITE_ENVIRONMENT/Daily_Fluences/.
19 Note that the 2MeV data set also considers contamination effects on the electron detectors on the
20 spacecrafts due to protons >32 MeV. Furthermore the 2MeV data is obtained from geostationary
21 satellites which perform in-situ measurements in the radiation belts and consequently do not
22 directly provide observations of precipitating particles. However, it is very likely that there is at
23 least a positive relation between 2MeV and precipitating relativistic radiation belt particles. Thus,
24 the 2MeV is not used as a proxy of precipitating particles but as an indicator of the influence from
25 the magnetosphere. Precipitating particle integral fluxes in polar regions are observed by sun-
26 synchronous Polar orbiting Operational Environmental Satellite (POES) detectors and the
27 corresponding data correlates better with geomagnetic indices than the GOES electron fluxes
28 (Sinnhuber et al., 2011). However, the respective measurements of the POES instruments tend to
29 underestimate the fluxes from ground-based observations during weak geomagnetic activity
30 (Rodger et al., 2013). Since this study focus on 2002 – 2011 and an essential part of this time
31 interval overlaps with low geomagnetic activity, GOES data and Ap are used instead of POES
32 measurements. The time series of all data sets are based on daily values, which were arithmetically

1 averaged to 26-day means centred at 1 April, 1 May, and 1 June. The means were separately
2 calculated for each index for the individual years from 2002 – 2011, however, 2MeV data are only
3 available until 2010.

4 **2.4 Numerical modelling**

5 The three-dimensional chemistry and transport model (3dCTM; Sinnhuber et al., 2012, appendix 1)
6 used here is based on the Bremen 3dCTM (e.g. Wissing et al., 2010), extending on 47 pressure
7 levels from the tropopause up to the lower thermosphere (~10 – 140 km) with a latitude/longitude
8 resolution of $2.5^\circ \times 3.75^\circ$. The model was recently updated with a variable H₂ and O₂ distribution,
9 leading to proper HO_x and consequently night time O₃ values at altitudes >60 km (see Sect. 1). The
10 3dCTM is driven by meteorological data obtained from simulations of the three-dimensional
11 dynamical model LIMA (Berger 2008) and the advection is calculated by applying the second-order
12 moments scheme reported by Prather (1986). In the stratosphere, a family approach for the chemical
13 families: O_x (O + O(¹D) + O₃), NO_x (N + NO + NO₂), HO_x (H + OH + HO₂), BrO_x (Br + BrO),
14 ClO_x (Cl + ClO + 2Cl₂O₂), and CHO_x (CH₃ + CH₃O₂ + CH₃OOH + CH₃O + HCO) is used, but was
15 not used for O_x, HO_x, and NO_x in the mesosphere/lower thermosphere region.

16 In this study the 3dCTM was used to investigate the impact of precipitating particles on O₃ inside
17 the Antarctic polar vortex at altitudes from 20 - 70 km. After a multi-year two-dimensional model
18 spin-up, two simulations from 2003 – 2009 were performed. The first run (base run) does not
19 consider any energetic particles, while the second run (EP run) includes ionisation effects by both
20 protons and electrons, using the ionisation rates provided by the Atmospheric Ionisation Module
21 Osnabrück (AIMOS; Wissing and Kallenrode 2009). The resulting NO_x production per created ion
22 pair includes various ionic and neutral reactions depending on the atmospheric background state
23 (Nieder et al., 2014). Simple parameterisations are used for the production of HO_x (Solomon et al.,
24 1981) and O (Porter et al., 1976). Note that heterogeneous chemistry was not included, which only
25 becomes important during spring in the lower stratosphere. Both model runs considered constant
26 solar minimum conditions ($F_{10.7} = 70 \cdot 10^{-22} \text{ W m}^{-2} \text{ Hz}^{-1}$) to exclude O₃ variations due to solar
27 activity. The obtained O₃ model results of both runs were separately selected according to the
28 vertical MIPAS retrieval grid for direct comparisons to the observations, repeating the described
29 algorithm to calculate the 26-day running means. Finally, in order to derive the O₃ vmr variations
30 solely originating from precipitating particles, the obtained averages of the base run were subtracted
31 from the corresponding O₃ values of the EP run. The results were divided by the arithmetic mean of
32 both runs and eventually multiplied by 100%.

1

2 **3 Results and discussion**

3 **3.1 Satellite observations**

4 **3.1.1 O₃ response from 2002 - 2011**

5 The 26-day O₃ vmr averages from 2002 - 2011 of each altitude-time interval (1 April – 1 November,
6 20 - 70 km) were individually grouped into years of high and low index activity. For this purpose
7 the index median of the corresponding time series of the 26-day average of an index (F10.7, Ap,
8 2MeV) centred around 1 April was calculated, only including years of actually available O₃
9 observations. Therefore the median of an index time series works as a threshold, dividing the entire
10 time interval from 2002-2011 in years of high (above the median) and low (below the median)
11 index activity. Note that the classification of the years does not only depend on the chosen index,
12 but due to data gaps also on the considered height-time interval as well as the instrument used.
13 Afterwards the arithmetic O₃ mean of the years of low index activity was subtracted from the O₃
14 mean of the years of high index activity, eventually dividing this absolute O₃ difference by the
15 arithmetic O₃ average of the entire observation period and multiplying the results by 100% for more
16 handy values. Thus the calculated relative O₃ difference (referred to as O₃ amplitude here)
17 represents the impact of the respective index on the O₃ background. To reduce the measurement
18 noise of the individual instruments, the results of all three instruments were merged by simply
19 calculating the arithmetic average but only if the corresponding O₃ amplitude of all three
20 instruments was available. Note that due to the major sudden stratospheric warming centred around
21 27 September (Azeem et al., 2010) the O₃ observations from 1 September - 1 November 2002 were
22 excluded. In contrast, the solar proton event in the end of October 2003 (Jackman et al., 2005) was
23 neglected due to its late occurrence. The performed analyses with O₃ observations, considering the
24 indices from 1 May and 1 June (not shown here), revealed no essential differences compared to 1
25 April or the structures became less obvious. Comparisons with earlier periods are not reasonable
26 because the vortex first builds up in April. Therefore the focus is set on the O₃ response to indices
27 centred around 1 April. The O₃ amplitude was calculated for ~~the~~ all three regions (CORE, EDGE,
28 and OUTSDIE) which were introduced in Sect. 2.1. The corresponding results reveal that the
29 pattern found inside the EDGE region are fairly similar and less noisy compared to the features
30 observed in the CORE area (not shown here). In contrast the O₃ amplitudes outside the Antarctic
31 polar vortex are fundamentally different. An example for the O₃ response associated to 1 April Ap in

1 the EDGE and the OUTSIDE region derived from MIPAS measurements is presented in Fig. 2,
2 showing considerably disagreeing structures and essentially weaker amplitudes, especially below 50
3 km. Thus comparison between the individual regions of the Southern Hemisphere ensures, that, the
4 pattern found in the EDGE region are actually originating from the Antarctic polar vortex.

5 Figure 3 displays the corresponding results of the O₃ amplitude from 2002 - 2011, but only for
6 values above the significance level of 95% while shaded areas show regions between the
7 significance level of 95% and 99%. The significance was calculated according to a Student's t-test,
8 based on the error of the mean of the 26-day running O₃ means and assuming the worst case
9 scenario of absolute error propagation. The MIPAS O₃ measurements (left column) reveal a high
10 negative response to Ap (upper row) in early Antarctic winter >60 km, on average ranging around
11 -10%. Further striking negative O₃ amplitudes occur in July between 30 and 40 km as well as
12 around 1 October at ~30 km, at least weakly indicating the downward transport of the Ap signal in
13 stratospheric O₃ due to NO_x predicted by model studies (e.g. Reddmann et al., 2010). In contrast, a
14 positive O₃ amplitude is found at the beginning of the winter between ~25 km and ~55 km (~10 –
15 20%), as well as at altitudes <30 km throughout the winter (up to ~20% in October at ~20 km) and
16 above the indicated subsiding layer of negative amplitudes. But considering that most of these
17 features drop below the significance level of 95% by combining the data of all three instruments
18 (right column), a more detailed investigation of these patterns is not reasonable. However, the
19 results of the merged data set show a well pronounced subsiding negative Ap signal from ~50 km in
20 June down to ~25 km in October, which is disrupted in August, while the generally positive
21 structures below 30 km are also still present.

22 The O₃ response to 2 MeV (middle row) derived from MIPAS observations also indicates a
23 downwelling of negative O₃ amplitudes, descending from ~60 km in June down to ~30 km in late
24 August. Additionally, the MIPAS O₃ response to 2MeV in early winter is reversed compared to the
25 corresponding influence from Ap on O₃, which does not originate from missing 2MeV data from
26 2011. Strong positive O₃ amplitudes are generally observed throughout the winter below 30 km,
27 exceeding values of ~20% in April and October, as well as during October between 30 km and 50
28 km where the maximum amplitude is lower (~10%). The positive features can be validated with the
29 composite results even if they are damped in the region below 30 km. However, this is not the case
30 for the negative response, except for a small area in June in the lower mesosphere. Considering that
31 the Ap responds to lower particle energy levels compared to 2MeV and that the behaviour of both
32 indices is essentially different from 2002 - 2010 (see Fig. 4), the different O₃ amplitudes associated
33 to Ap and 2MeV are still reasonable.

1 The O_3 response to F10.7 (lowermost row) is fairly similar between MIPAS and the merged
2 measurements, and both also agree with the respective pattern observed for Ap, including the
3 indicated downwelling of negative O_3 amplitudes during midwinter from 50 to 25 km. The
4 composite O_3 shows strong positive amplitudes in May >55 km which originate from SMR
5 measurements and are most likely due to the low vertical resolution of the SMR instrument at these
6 altitudes (see Sect. 2.2.3). The high agreement between the results of Ap/ O_3 and F10.7/ O_3 might
7 originate from the coupling of both indices during solar maximum years (Gray et al., 2010, their
8 Fig. 1). In order to investigate a possible cross-correlation between solar radiation and geomagnetic
9 disturbances, the analysis was repeated for years of moderate solar activity, only including 2005 –
10 2010 (Fig. 4). Similar analyses to extract a more distinct solar signal during times of approximately
11 constant geomagnetic activity were not reasonable, because the respective years of nearly constant
12 Ap values (2002, 2005, 2006, 2008, 2010) do not provide a sufficient amount of data in MIPAS and
13 SMR measurements.

14 **3.1.2 O_3 behaviour during solar minimum activity (2005 - 2010)**

15 Figure 5 displays the obtained O_3 amplitudes for solar quiet times (2005 – 2010) associated to 1
16 April Ap, again only showing values above 95% significance level and shading the area of regions
17 between 95% and 99%. The MIPAS O_3 response to Ap indicates a subsiding negative signal (~-10
18 to -15%), starting in late June slightly below 50 km and propagating downwards to ~25 km
19 throughout the winter. However, the middle part of the downwelling between late July and late
20 September is below the significance level of 95% and therefore not shown here. Furthermore, the
21 hinted subsidence is closely surrounded by well pronounced positive O_3 amplitudes, especially
22 below ~30 km which maximise in September (>20%). There is also a negative structure centred at 1
23 June at ~60 km, which cannot be caused by NO_x but most likely results from HO_x formation (see
24 Sect. 1). Considering the composite results, the downwelling Ap signal in O_3 becomes apparent and
25 robust but slightly weaker (~-10%) while the positive features are also damped but still present. The
26 mesospheric response is generally weak and the high positive O_3 amplitudes in May are again
27 caused by the SMR measurements.

28 The 2MeV impact on MIPAS O_3 shows generally agreeing features with the influence of the
29 geomagnetic activity and is also of similar magnitude, however, the downwelling negative signal is
30 hinted to already start in late May at ~55 km. In contrast to the O_3 response to Ap, the downwards
31 propagating 2MeV signal is less robust and can be only guessed in the composite O_3 amplitude,
32 while the positive structures (~10 - 15%) in August below 30 km and in September between 30 km

1 and 50 km are still present. In general, the 2MeV features are less obvious in the O₃ composite,
2 except for the positive O₃ amplitudes above the hinted downward transport. Nevertheless, the
3 agreement between Ap and 2MeV pattern is quite strong, in MIPAS observations in particular,
4 although both parameters are only indirectly related to O₃. However, the O₃ structure
5 associated feedback to both indices is far too similar and additionally found in all three instruments
6 to be a coincidence, even if the descending O₃ response to 2 MeV is weaker. Since Ap represents
7 lower particle energy levels compared to the 2MeV and both indices are only moderately correlated
8 (see Fig. 4), the similar results That strongly indicates a related source mechanism, suggesting solar
9 wind variability.

10 Considering the entire process, that energetic particles produce NO_x which eventually destroys
11 stratospheric O₃, the Ap impact observed in O₃ (see Fig. 5) is expected to be reversed in NO_x, at
12 least in the stratosphere. In order to investigate this in more detail, the analysis was repeated for 1
13 April Ap and NO_x. Here NO_x is represented only by NO₂ from MIPAS observations, because the
14 respective NO measurements are quite noisy compared to NO₂, especially below 30 km. This is still
15 reasonable because NO is converted to NO₂ during night and therefore NO₂ is the major fraction of
16 NO_x inside the Antarctic polar vortex. The corresponding results include the years 2005 – 2010 and
17 are displayed in Fig. 6, supporting that the stratospheric O₃ depletion can be indeed associated to the
18 catalytic NO_x/O₃ cycle. The Ap signal in NO₂ is stronger by the factor of 2 - 5, compared to the
19 respective O₃ amplitudes. The sharp gradient in mid July originates from 2005 NO₂ data, which are
20 not available afterwards. However, the general structure of the subsiding Ap signal in NO₂ is still
21 similar with and without 2005 observations. Note that the essentially smaller NO₂ amplitudes in
22 October below the significance level of 95% are not in conflict with the respective well pronounced
23 negative O₃ response, because the latter one results from an accumulation effect from the NO₂
24 above. Furthermore, large negative NO₂ amplitudes throughout the entire winter below ~30 km are
25 observed, matching the high positive O₃ responsefeedbacks to Ap. A possible reason for this
26 behaviour might be that NO₂ is stored in reservoir species, like ClONO₂, and HNO₃, and N₂O₅, due
27 to reactions with ClO₂, and OH, and NO₃, respectively. However, N₂O₅ is converted to HNO₃ via
28 water ion cluster chemistry (López-Puertas et al., 2005, their reactions 1 and 8 – 12), which was
29 also investigated with respect to EPP for conditions without solar proton events by Stiller et al.
30 (2005). These reactions—This eventually leads to lower NO_x concentrations, and consequently
31 slowings down the catalytic O₃ depletion. Based on the corresponding MIPAS climatologies (not
32 shown here), HNO₃ is more important until mid July, while ClONO₂ is dominating afterwards and
33 its influence becomes essentially crucial in spring due to heterogeneous chemistry which has taken

place before. This suggested NO₂-ClONO₂ mechanism is supported by Whole Atmosphere Community Climate Model results reported by Jackman et al. (2009, their Fig. 6 and 7), who simulated the impact of the SPE in July 2000 on stratospheric O₃ and NO_y (= NO_x + NO₃ + N₂O₅ + HNO₃ + HO₂NO₂ + ClONO₂ + BrONO₂).

Furthermore, the positive O₃ amplitudes below ~30 km could be also partly explained by the self healing effect of O₃ (Jackman and McPeters, 1985). Altitude regions of reduced O₃ will lead to increased solar UV radiation in the layers directly below. This is accompanied by a higher production of atomic oxygen and would consequently increase the formation of O₃. However, this proposed mechanism would only have an additional effect, contributing to the formation of O₃ in the atmospheric layer right below the subsidence, but cannot account for the entire region. Note that this layer is also present throughout the entire winter, and thus an influence from the vortex above is unlikely but any further investigations are beyond the scope of this study.

Additionally, the area of high positive Ap/O₃ structure between 35 km and 50 km from August - September cannot be completely explained by the NO_x/O₃ cycle. In detail~~However~~, the respective Ap influence of NO₂ is close to 0 and consequently well below the 95%, while the respective MIPAS ClONO₂ amplitude (not shown here) reveals positive values, which are also mostly below the 95% significance level. These results aresignificance level and is therefore at least not in conflict with a higher O₃ ~~amplituder~~response. Furthermore, this positive Ap impact on O₃ is essentially less visible in the composite results than in MIPAS data, and a corresponding composite analysis for Ap/NO₂ is necessary for a more detailed investigation. But this is not possible due to non-existing NO₂ measurements from SABER and SMR. Thus no definite explanation can be given at this state and this feature is a subject of a future work. However, it should be pointed out that this structure does not harm the underlying mechanism proposed to explain the identified negative O₃ amplitude and subsequent downward transport.

3.2 Comparison with 3dCTM

The simulated O₃ amplitude between the EP run and base run, representing high and low geomagnetic activity, respectively, is displayed in Fig. 7. Note that the modelled O₃ amplitude is also referred to as O₃ amplitude here, which is justified because “observed” and “modelled” O₃ amplitude still hold the same physical meaning, even if the calculation algorithm is slightly different. It is reasonable to investigate the complete simulated time interval from 2003 – 2009, because the model runs represent solar minimum conditions similar to the years 2005 - 2010. The results reveal apparent negative O₃ amplitudes propagating downwards throughout the winter with

1 maximum negative values during midwinter between 45 km and 60 km. The subsidence shows
2 larger negative O₃ amplitudes compared to the measurements and is also much broader, which
3 might be due to the constant F10.7 and the prescribed dynamics, both reducing the inter-annual
4 variability of O₃. Furthermore, we performed an on/off experiment, while in reality the EEP indirect
5 effect is a persistent feature. Below 30 km the observed high positive O₃ amplitudes associated to
6 Ap are only indicated in the model results by essentially weaker and additionally negative
7 amplitudes. However, the model amplitudes are at least less negative compared to the values above.
8 The second positive region above the downwelling is completely missing. Further note that the
9 strong positive [responsefeedback](#) during late winter/early spring below 30 km might not be
10 reproduced by the model due to missing heterogeneous chemistry. The proposed self healing effect
11 of O₃ (see Sect 3.1.2) was also tested, using O¹D as a proxy for the O₃ photolysis rate in the Lyman-
12 alpha band and calculating the O¹D amplitude (not shown here). However, the expected positive
13 response directly below the downwelling is only partly visible and even below the 67% significance
14 level.

15 The qualitative agreement between model results and observations in the stratosphere suggests that
16 the subsiding Ap signal found in O₃ is actually originating from particle precipitation. However, the
17 simulated downwelling starts at altitudes >60 km while observations reveal no obvious structures in
18 the mesosphere, possibly caused by satellite sampling. As already stated in Sect 3.1.2, the
19 mesospheric behaviour cannot be caused by NO_x, because the NO_x/O₃ cycle is not efficiently
20 working at these altitudes. Thus the O₃ depletion >50 km could be accounted to OH production,
21 which is most likely overestimated in the model and consequently leads to an increased O₃
22 depletion not observed by the satellite instruments.

23

24 **4 Conclusions**

25 We have investigated the O₃ behaviour inside the Antarctic polar vortex from 2002 - 2011, observed
26 by three independent satellite based instruments ENVISAT/MIPAS, Odin/SMR, and
27 TIMED/SABER. These O₃ vmr measurements, based on 26-day running means from 1 April – 1
28 November covering altitudes from 20 – 70 km, were individually grouped into high and low index
29 activity according to the 26-day averages centred around 1 April, 1 May, and 1 June of different
30 solar and geomagnetic indices (F10.7, Ap, 2MeV). After minimising the direct influence of the solar
31 radiation by only considering the period of solar minimum activity from 2005 – 2010 we found a
32 negative O₃ response caused by geomagnetic activity (Ap) from 1 April in all three instruments,
33 ranging from -5% to -10% and propagating downwards throughout the Antarctic winter from ~50

1 km down to ~25 km. This subsiding negative signal in O₃ is above the significance level of 95% and overlaps with the corresponding positive NO₂ response to 1 April Ap, supporting that NO_x is indeed the cause of the O₃ depletion. We could also show that the high positive O₃ [responsefeedback](#) below 30 km, which is present during the entire winter, is in agreement with respective negative NO₂ structures. The cause of the NO₂ behaviour is possibly related to the formation of the reservoir species ClONO₂ and HNO₃, slowing down the catalytic destruction of O₃ by Cl. The O₃ pattern induced by the magnetosphere (2MeV) from 1 April are similar but weaker, compared to the respective geomagnetic activity, still suggesting a related source mechanism between 2MeV and Ap like solar wind variability. The composite observations of all three instruments are in good qualitative agreement with 3dCTM simulation, revealing similar O₃ pattern induced by the geomagnetic activity from 1 April while the simulated O₃ response is larger but still in the same order of magnitude.

13 However, we have to point out that the validity of the subsiding O₃ depletion associated to geomagnetic activity and NO_x is not ensured due to the short time series of only 6 years at most. Thus, we conclude that precipitating particles are strongly indicated as a factor contributing to stratospheric O₃ during Antarctic winter, but we cannot prove the link unambiguously.

18 **Authors' contribution**

19 T. F. analysed the satellite and indices data and wrote the final script. G. S., J. U.+K. P., and M. M. provided the O₃ data from ENVISAT/MIPAS, Odin/SMR, and TIMED/SABER, respectively, and all of them contributed to interpretation. H. N. performed the 3dCTM simulations. M. S. initiated the study and contributed to interpretation.

24 **Acknowledgements**

25 T. Fytterer, H. Nieder, and M. Sinnhuber gratefully acknowledge funding by the Helmholtz Association of German Research Centres (HGF), grant VH-NG-624. The authors also acknowledge support by Deutsche Forschungsgemeinschaft and Open Access Publishing Fund of Karlsruhe Institute of Technology. Odin is a Swedish-led satellite project funded jointly by the Swedish National Space Board (SNSB), the Canadian Space Agency (CSA), the National Technology Agency of Finland (Tekes), the Centre National d'Etudes Spatiales (CNES) in France and the third party mission program of the European Space Agency (ESA). We further like to thank the ERA-

1 Interim for free provision of data and related support.

2

3 **References**

- 4 Azeem, S. M. I., Talaat, E. R., Sivjee, G. G., and Yee, J. H.: Mesosphere and lower thermosphere
5 anomalies during the 2002 Antarctic stratospheric warming event, *Ann. Geophys.*, 28, 267-276,
6 doi:10.5194/angeo-28-267-2010, 2010.
- 7 Berger, U.: Modeling of middle atmosphere dynamics with LIMA, *J. Atmos. Sol-Terr. Phys.*, 70,
8 1170–1200, doi:10.1016/j.jastp.2008.02.004, 2008.
- 9 Eckert, E., von Clarmann, T., Kiefer, M., Stiller, G. P., Lossow, S., Glatthor, N., Degenstein, D. A.,
10 Froidevaux, L., Godin-Beekmann, S., Leblanc, T., McDermid, S., Pastel, M., Steinbrecht, W.,
11 Swart, D. P. J., Walker, K. A., and Bernath, P. F.: Drift-corrected trends and periodic variations in
12 MIPAS IMK/IAA ozone measurements, *Atmos. Chem. Phys.*, 14, 2571-2589, doi:10.5194/acp-14-
13 2571-2014, 2014.
- 14 Fischer, H., Birk, M., Blom, C., Carli, B., Carlotti, M., von Clarmann, T., Delbouille, L., Dudhia,
15 A., Ehhalt, D., Endemann, M., Flaud, J. M., Gessner, R., Kleinert, A., Koopman, R., Langen, J.,
16 López-Puertas, M., Mosner, P., Nett, H., Oelhaf, H., Perron, G., Remedios, J., Ridolfi, M., Stiller, G.
17 P., and Zander, R.: MIPAS: an instrument for atmospheric and climate research, *Atmos. Chem.*
18 *Phys.*, 8, 2151–2188, doi:10.5194/acp-8-2151-2008, 2008.
- 19 Funke, B., López-Puertas, M., von Clarmann, T., Stiller, G. P., Fischer, H., Glatthor, N., Grabowski,
20 U., Höpfner, M., Kellmann, S., Kiefer, M., Linden, A., Mengistu Tsidu, G., Milz, M., Steck, T., and
21 Wang, D. Y.: Retrieval of stratospheric NO_x from 5.3 and 6.2 μm nonlocal thermodynamic
22 equilibrium emissions measured by Michelson Interferometer for Passive Atmospheric Sounding
23 (MIPAS) on Envisat, *J. Geophys. Res.*, 110, D09302, doi:10.1029/2004JD005225, 2005.
- 24 Funke, B., Baumgaertner, A., Calisto, M., Egorova, T., Jackman, C. H., Kieser, J., Krivolutsky, A.,
25 López-Puertas, M., Marsh, D. R., Reddmann, T., Rozanov, E., Salmi, S.-M., Sinnhuber, M., Stiller,
26 G. P., Verronen, P. T., Versick, S., von Clarmann, T., Vyushkova, T. Y., Wieters, N., and Wissing, J.
27 M.: Composition changes after the “Halloween” solar proton event: the High Energy Particle
28 Precipitation in the Atmosphere (HEPPA) model versus MIPAS data intercomparison study, *Atmos.*
29 *Chem. Phys.*, 11, 9089–9139, doi:10.5194/acp-11-9089-2011, 2011.
- 30 Funke, B., López-Puertas, M., Stiller, G. P., and von Clarmann, T.: Mesospheric and stratospheric
31 NO_y produced by energetic particle precipitation during 2002–2012, *J. Geophys. Res-Atmos.*, 119,

1 4429-4446, doi:10.1002/2013JD021404, 2014.

2 Glatthor, N., von Clarmann, T., Fischer, H., Funke, B., Gil-López, S., Grabowski, U., Höpfner, M.,
3 Kellmann, S., Linden, A., López-Puertas, M., Mengistu Tsidu, G., Milz, M., Steck, T., Stiller, G. P.,
4 and Wang, D. Y.: Retrieval of stratospheric ozone profiles from MIPAS/ENVISAT limb emission
5 spectra: a sensitivity study, *Atmos. Chem. Phys.*, 6, 2767–2781, doi:10.5194/acp-6-2767-2006,
6 2006.

7 Gray, L. J., Beer, J., Geller, M., Haigh, J. D., Lockwood, M., Matthes, K., Cubasch, U., Fleitmann,
8 D., Harrison, G., Hood, L., Luterbacher, J., Meehl, G. A., Shindell, D., van Geel, B., and White, W.:
9 Solar influences on climate, *Rev. Geophys.*, 48, RG4001, doi:10.1029/2009RG000282, 2010.

10 Jackman C. H., and McPeters, R. D.: The Response of Ozone to Solar Proton Events During Solar
11 Cycle 21: A Theoretical Interpretation, *J. Geophys. Res.*, 90, 7955-7966, 1985.

12 Jackman, C. H., DeLand, M. T., Labow, G. J., Fleming, E. L., Weisenstein, D. K., Ko, M. K. W.,
13 Sinnhuber, M., and Russell III, J. M.: Neutral atmospheric influences of the solar proton events in
14 October--November 2003, *J. Geophys. Res.*, 110, A09S27, doi:10.1029/2004JA010888, 2005.

15 [Jackman, C. H., Marsh, D. R., Vitt, F. M., Garcia, R. R., Randall, C. E., Fleming, E. L., and Frith, S.](#)
16 [M.: Long-term middle atmospheric influence of very large solar proton events, *J. Geophys. Res.*,](#)
17 [114, D11304, doi:10.1029/2008JD011415, 2009.](#)

18 Lary, D. J.: Catalytic destruction of stratospheric ozone, *J. Geophys. Res.*, 102, 21515-21526,
19 doi:10.1029/97JD00912, 1997.

20 López-Puertas, M., Funke, B., Gil-López, S., von Clarmann, T., Stiller, G. P., Höpfner, M.,
21 Kellmann, S., Mengistu Tsidu, G., Fischer, H., and Jackman, C. H.: HNO₃, N₂O₅, and ClONO₂
22 enhancements after the October–November 2003 solar proton events, *J. Geophys. Res.*, 110,
23 A09S44, doi:10.1029/2005JA011051, 2005.

24 Murtagh, D., Frisk, U., Merino, F., Ridal, M., Jonsson, A., Stegman, J., Witt, G., Eriksson, P.,
25 Jiménez, C., Megie, G., de la Noë, J., Ricaud, P., Baron, P., Pardo, J. R., Hauchcorne, A.,
26 Llewellyn, E. J., Degenstein, D. A., Gattinger, R. L., Lloyd, N. D., Evans, W. F. J., McDade, I. C.,
27 Haley, C. S., Sioris, C., von Savigny, C., Solheim, B. H., McConnell, J. C., Strong, K., Richardson,
28 E. H., Leppelmeier, G. W., Kyrölä, E., Auvinen, H., and Oikarinen, L.: An overview of the Odin
29 atmospheric mission, *Can. J. Phys.*, 80, 309-319, doi:10.1139/p01-157, 2002.

30 Nash, E. R., Newman, P. A., Rosenfield, J. E., and Schoeberl, M. R.: An objective determination of
31 the polar vortex using Ertel's potential vorticity, *J. Geophys. Res.*, 101, 9471-9478,

1 doi:10.1029/96JD00066, 1996.

2 Nieder, H., Winkler, H., Marsh, D. R., and Sinnhuber, M.: NO_x production due to energetic particle
3 precipitation in the MLT region: Results from ion chemistry model studies, *J. Geophys. Res-Space.*,
4 119, 2137-2148, doi:10.1002/2013JA019044, 2014.

5 Porter, H. S., Jackman, C. H., and Green, A. E. S.: Efficiencies for production of atomic nitrogen and
6 oxygen by relativistic proton impact in air, *J. Chem. Phys.*, 65, 154–167, doi:10.1063/1.432812,
7 1976.

8 Prather, M.: Numerical advection by conservation of second-order moments, *J. Geophys. Res.*, 91,
9 6671-6681, doi:10.1029/JD091iD06p06671, 1986.

10 Preusse, P., Eckermann, S. D., Ern, M., Oberheide, J., Picard, R. H., Roble, R. M., Riese, M.,
11 Russell III, J. M., and Mlynczak, M. G.: Global ray tracing simulations of the SABER gravity wave
12 climatology, *J. Geophys. Res.*, 114, D08126, doi:10.1029/2008JD011214, 2009.

13 Randall, C. E., Rusch, D. W., Bevilacqua, R. M., and Hoppel, K. W.: Polar Ozone And Aerosol
14 Measurement (POAM) II stratospheric NO₂, 1993-1996, *J. Geophys. Res.*, 103, 28361-28371,
15 doi:10.1029/98JD02092, 1998.

16 Randall, C. E., Harvey, V. L., Singleton, C. S., Bailey, S. M., Bernath, P. F., Codrescu, M.,
17 Nakajima, H., and Russell III, J. M.: Energetic particle precipitation effects on the Southern
18 Hemisphere stratosphere in 1992–2005, *J. Geophys. Res.*, 112, D08308,
19 doi:10.1029/2006JD007696, 2007.

20 Reddmann, T., Ruhnke, R., Versick, S., and Kouker, W.: Modeling disturbed stratospheric chemistry
21 during solar-induced NO_x enhancements observed with MIPAS/ENVISAT, *J. Geophys. Res.*, 115,
22 D00I11, doi:10.1029/2009JD012569, 2010.

23 Rodger, C. J., A. J. Kavanagh, M. A. Clilverd, and S. R. Marple: Comparison between POES
24 energetic electron precipitation observations and riometer absorptions: Implications for determining
25 true precipitation fluxes, *J. Geophys. Res. Space Physics*, 118, 7810–7821,
26 doi:10.1002/2013JA019439, 2013.

27 Rong, P. P., Russell III, J. M., Mlynczak, M. G., Remsberg, E. E., Marshall, B. T., Gordley, L. L.,
28 and López-Puertas, M.: Validation of Thermosphere Ionosphere Mesosphere Energetics and
29 Dynamics/Sounding of the Atmosphere using Broadband Emission Radiometry (TIMED/SABER)
30 v1.07 ozone at 9.6 μm in altitude range 15–70 km, *J. Geophys. Res.*, 114, D04306,
31 doi:10.1029/2008JD010073, 2009.

- 1 Rusch, D. W., Gerard, J. C., Solomon, S., Crutzen, P. J., and Reid, G. C.: The effect of particle
2 precipitation events on the neutral and ion chemistry of the middle atmosphere—I. Odd nitrogen,
3 Planet. Space Sci., 29, 767–774, doi:10.1016/0032-0633(81)90048-9, 1981.
- 4 [Sinnhuber, M., S. Kazeminejad, and J. M. Wissing, Interannual variation of NO_x from the lower
5 thermosphere to the upper stratosphere in the years 1991–2005, J. Geophys. Res., 116, A02312,
6 doi:10.1029/2010JA015825, 2011.](#)
- 7 Sinnhuber, M., Nieder, H., and Wieters, N.: Energetic particles precipitation and the chemistry of
8 the mesosphere/lower thermosphere, Surv. Geophys., 33, 1281–1334, doi:10.1007/s10712-9201-3,
9 2012.
- 10 Solomon, S., Rusch, D. W., Gerard, J. C., Reid, G. C., and Crutzen, P. J.: The effect of particle
11 precipitation events on the neutral and ion chemistry of the middle atmosphere: II. odd hydrogen,
12 Planet. Space Sci., 29, 885–892, doi:10.1016/0032-0633(81)90078-7, 1981.
- 13 Solomon, S., Crutzen, P. J., and Roble, R. G.: Photochemical coupling between the thermosphere
14 and the lower atmosphere 1. odd nitrogen from 50 to 120 km, J. Geophys. Res., 87, 7206–7220,
15 doi:10.1029/JC087iC09p07206, 1982.
- 16 Steck, T., von Clarmann, T., Fischer, H., Funke, B., Glatthor, N., Grabowski, U., Höpfner, M.,
17 Kellmann, S., Kiefer, M., Linden, A., Milz, M., Stiller, G. P., Wang, D. Y., Allaart, M.,
18 Blumenstock, T., von der Gathen, P., Hansen, G., Hase, F., Hochschild, G., Kopp, G., Kyrö, E.,
19 Oelhaf, H., Raffalski, U., Redondas Marrero, A., Remsberg, E., Russell III, J. M., Stebel, K.,
20 Steinbrecht, W., Wetzell, G., Yela, M., and Zhang, G.: Bias determination and precision validation of
21 ozone profiles from MIPAS-Envisat retrieved with the IMK-IAA processor, Atmos. Chem. Phys., 7,
22 3639–3662, doi:10.5194/acp-7-3639-2007, 2007.
- 23 [Stiller, G. P., G. M. Tsidu, T. von Clarmann, N. Glatthor, M. Höpfner, S. Kellmann, A. Linden, R.
24 Ruhnke, H. Fischer, M. López-Puertas, B. Funke, and S. Gil-López: An enhanced HNO₃ second
25 maximum in the Antarctic midwinter upper stratosphere 2003, J. Geophys. Res., 110, D20303,
26 doi:10.1029/2005JD006011, 2005.](#)
- 27 Urban, J., Lautié, N., Le Flochmoën, E., Jiménez, C., Eriksson, P., de La Noë, J., Dupuy, E.,
28 Ekström, M., El Amraoui, L., Frisk, U., Murtagh, D., Olberg, M., and Ricaud, P.: Odin/SMR limb
29 observations of stratospheric trace gases: Level 2 processing of ClO, N₂O, HNO₃, and O₃, J.
30 Geophys. Res., 110, D14307, doi:10.1029/2004JD005741, 2005.
- 31 Von Clarmann, T., Glatthor, N., Grabowski, U., Höpfner, M., Kellmann, S., Kiefer, M., Linden, A.,

1 Mengistu Tsidu, G., Milz, M., Steck, T., Stiller, G. P., Wang, D. Y., Fischer, H., Funke, B., Gil-
2 López, S., and López-Puertas, M.: Retrieval of temperature and tangent altitude pointing from limb
3 emission spectra recorded from space by the Michelson Interferometer for Passive Atmospheric
4 Sounding (MIPAS), *J. Geophys. Res.*, 108(D23), 4736, doi:10.1029/2003JD-003602, 2003.

5 Von Clarmann, T., Höpfner, M., Kellmann, S., Linden, A., Chauhan, S., Funke, B., Grabowski, U.,
6 Glatthor, N., Kiefer, M., Schieferdecker, T., Stiller, G. P., and Versick, S.: Retrieval of temperature,
7 H₂O, O₃, HNO₃, CH₄, N₂O, ClONO₂ and ClO from MIPAS reduced resolution nominal mode limb
8 emission measurements, *Atmos. Meas. Tech.*, 2, 159-175, doi:10.5194/amt-2-159-2009, 2009.

9 Wissing, J. M. and Kallenrode, M. B.: Atmospheric Ionization Module Osnabrück (AIMOS): a 3-D
10 model to determine atmospheric ionization by energetic charged particles from different
11 populations, *J. Geophys. Res.*, 114, A06104, doi:10.1029/2008JA013884, 2009.

12 Wissing, J. M., Kallenrode, M. B., Wieters, N., Winkler, H., and Sinnhuber, M.: Atmospheric
13 Ionization Module Osnabrück (AIMOS): 2. Total particle inventory in the October–November 2003
14 event and ozone, *J. Geophys. Res.*, 115, A02308, doi:10.1029/2009JA014419, 2010.

15
16
17
18
19
20
21
22
23
24
25
26
27
28
29

1 Table 1. Limits, derived from the potential vorticity ($10^{-6} \text{ K m}^2 \text{ s}^{-1} \text{ kg}^{-1}$), of the southern hemispheric
2 regions CORE, EDGE, and OUTSIDE at the individual heights. The altitudes are adapted from the
3 MIPAS retrieval grid and the shown potential vorticity values hold for 2002 – 2011.

nominal height (km)	CORE	EDGE	OUTSIDE	nominal height (km)	CORE	EDGE	OUTSIDE
20	-60	-50	-30	37	-3600	-1900	-1000
21	-70	-50	-30	38	-6000	-2500	-1500
22	-90	-70	-40	39	-6000	-3000	-2000
23	-150	-90	-40	40	-9000	-3500	-2000
24	-200	-100	-60	41	-9000	-4000	-2000
25	-180	-110	-60	42	-9000	-4000	-2000
26	-280	-160	-100	43	-15000	-5000	-3000
27	-360	-220	-120	44	-15000	-5500	-3000
28	-600	-250	-120	46	-22000	-8000	-4000
29	-900	-300	-150	48	-18000	-10000	-2000
30	-800	-400	-200	50	-36000	-12000	-4000
31	-1000	-400	-200	52	-32000	-16000	-4000
32	-1600	-600	-300	54	-36000	-16000	-4000
33	-2000	-800	-400	56	-60000	-30000	-5000
34	-1800	-1100	-400	58	-60000	-30000	-10000
35	-2800	-1400	-800	60	-60000	-30000	-10000
36	-4000	-1600	-1000	62 – 70	-180000	-90000	-30000

5
6
7
8
9
10
11
12
13
14
15

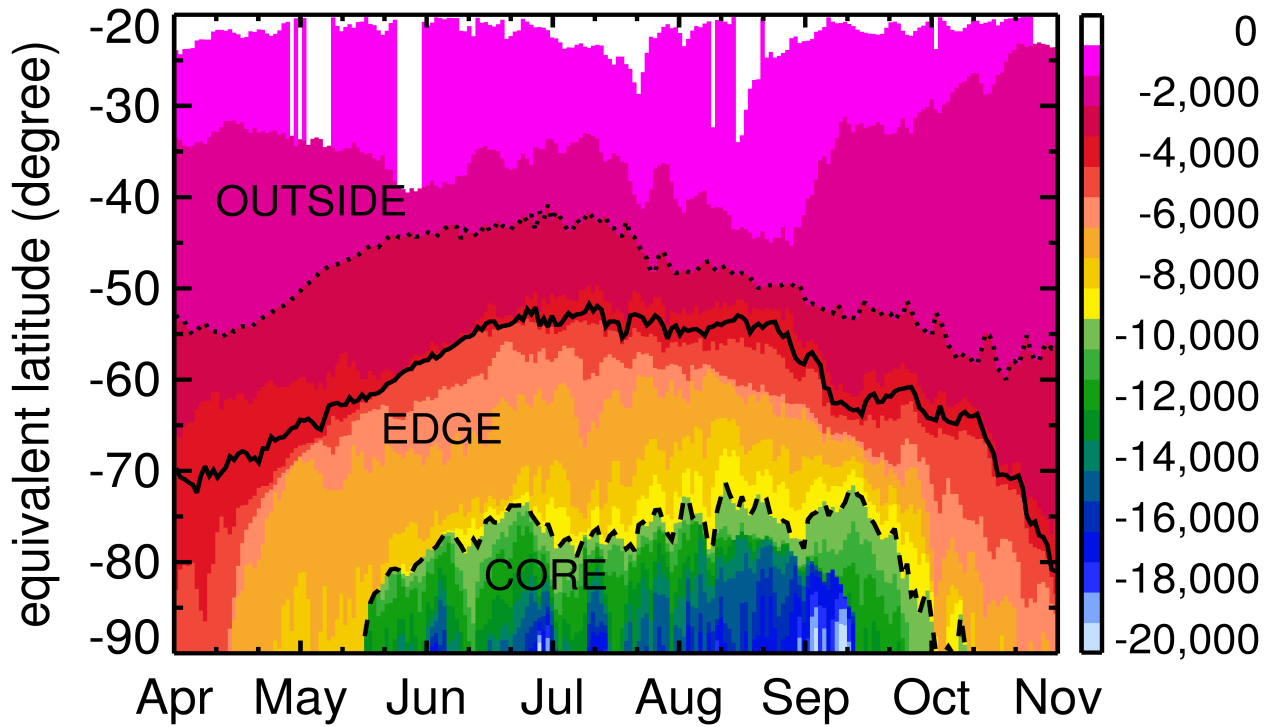
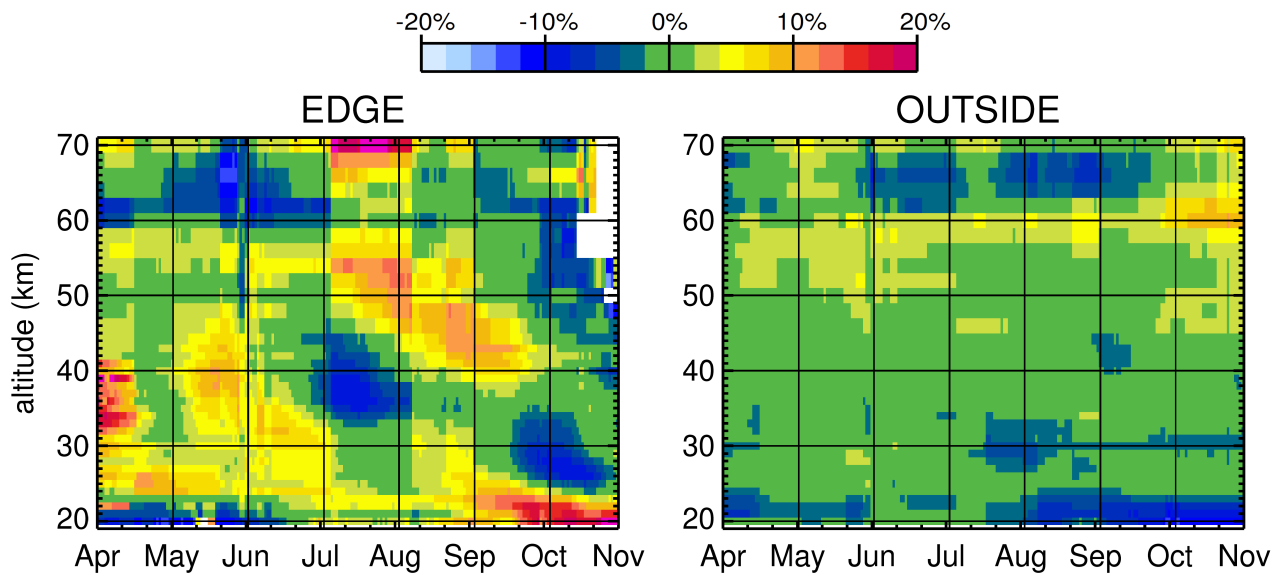
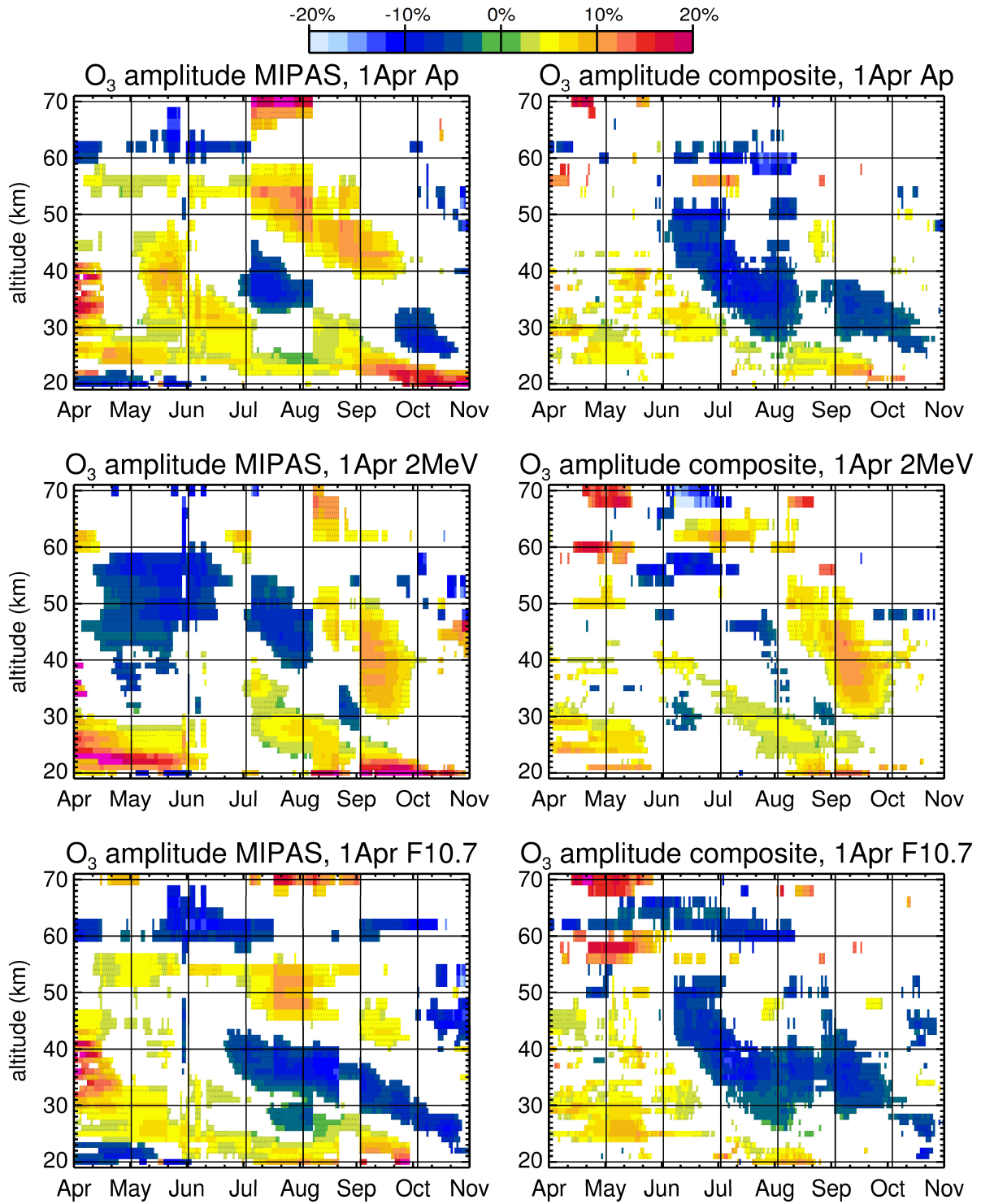


Figure 1. Potential vorticity (10^{-6} K m² s⁻¹ kg⁻¹, colour scale) at ~40 km during the Antarctic winter 2011 as a function of time and equivalent latitude. The thresholds of the regions OUTSIDE (dotted line), EDGE (solid line) and CORE (dashed line) are included. Potential vorticity was calculated from ECMWF Era-Interim data.



1
2 Figure 2. Example of the O₃ amplitude (see Sect. 3.1.1 for definition) observed by MIPAS from
3 2002 – 2011 between years of high Ap index and years of low Ap index centred around 1 April, for
4 the regions EDGE (left) and OUTSIDE (right).



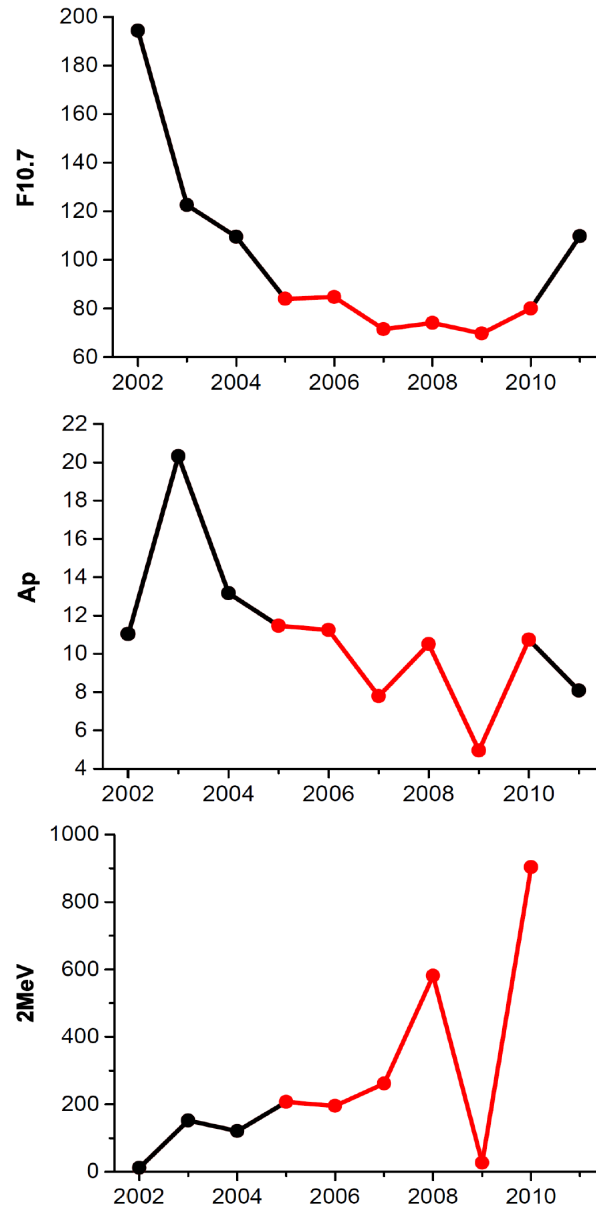
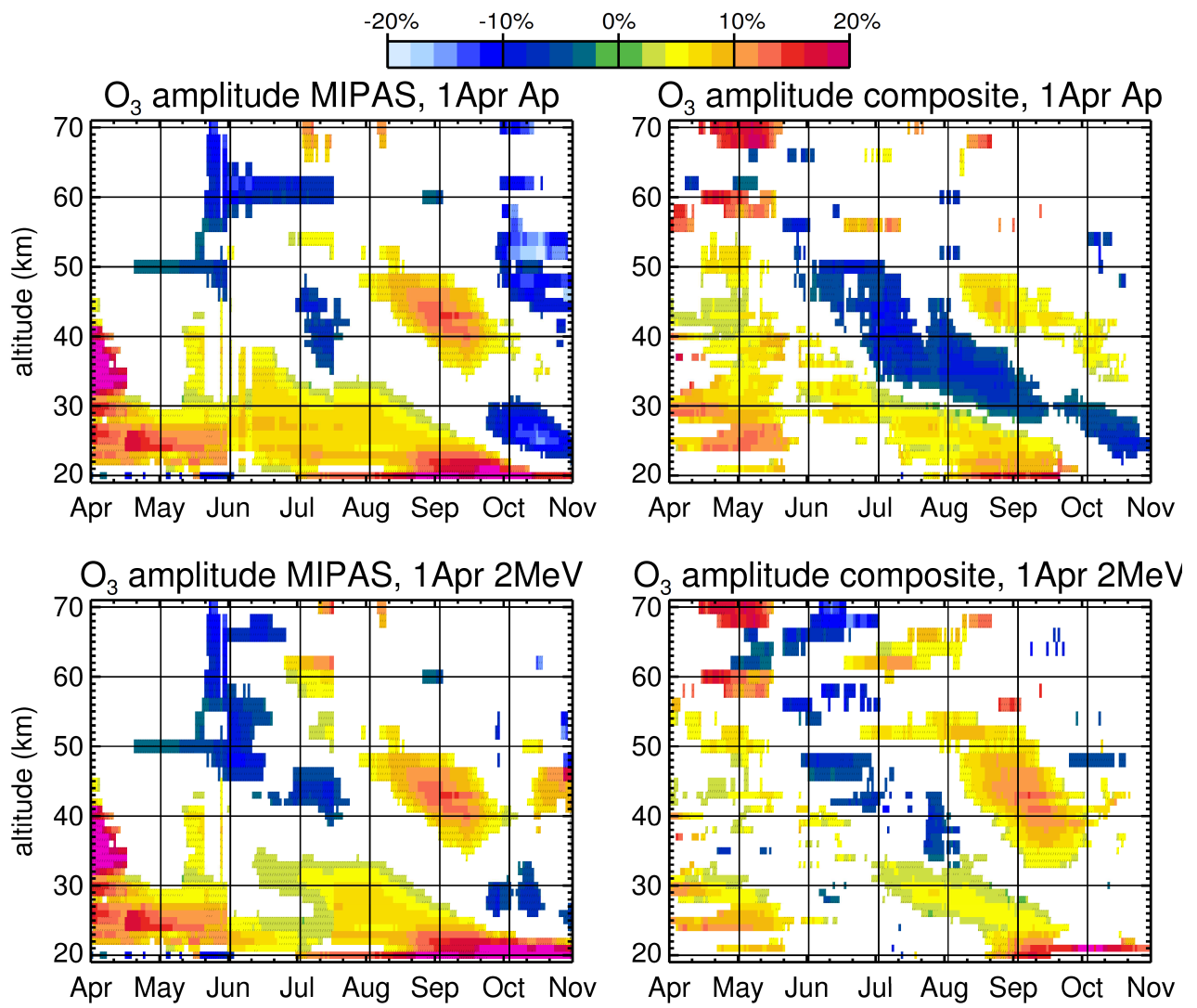
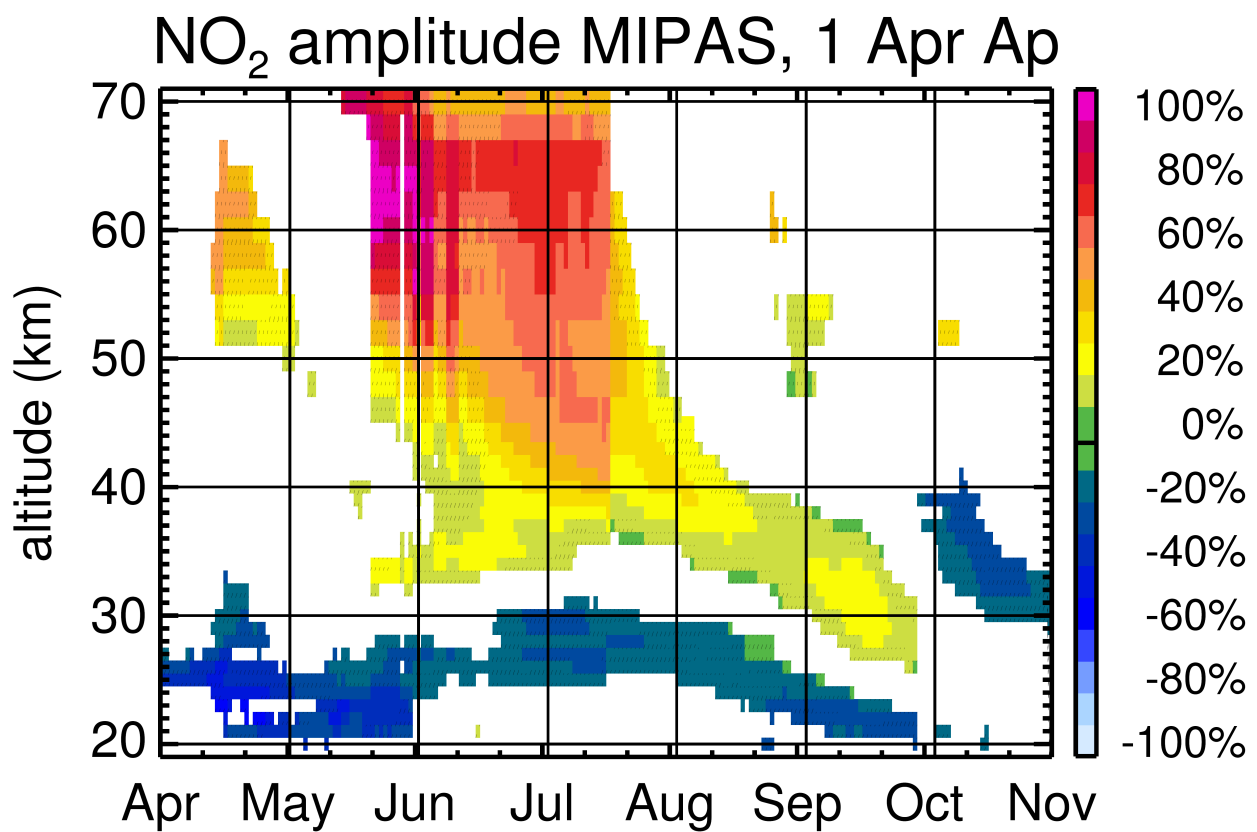


Figure 4. Time series from 2002 – 2011 of the 26-day averages centred around 1 April of the F10.7 cm solar radio flux ($10^{-22} \text{ W m}^{-2} \text{ Hz}^{-1}$, top), Ap index (middle), and $\geq 2 \text{ MeV}$ electron flux (electrons $\text{cm}^{-2} \text{ day}^{-1} \text{ sr}^{-1}$, bottom). The period of low solar activity from 2005 – 2010 is marked in red. Note the different scaling.

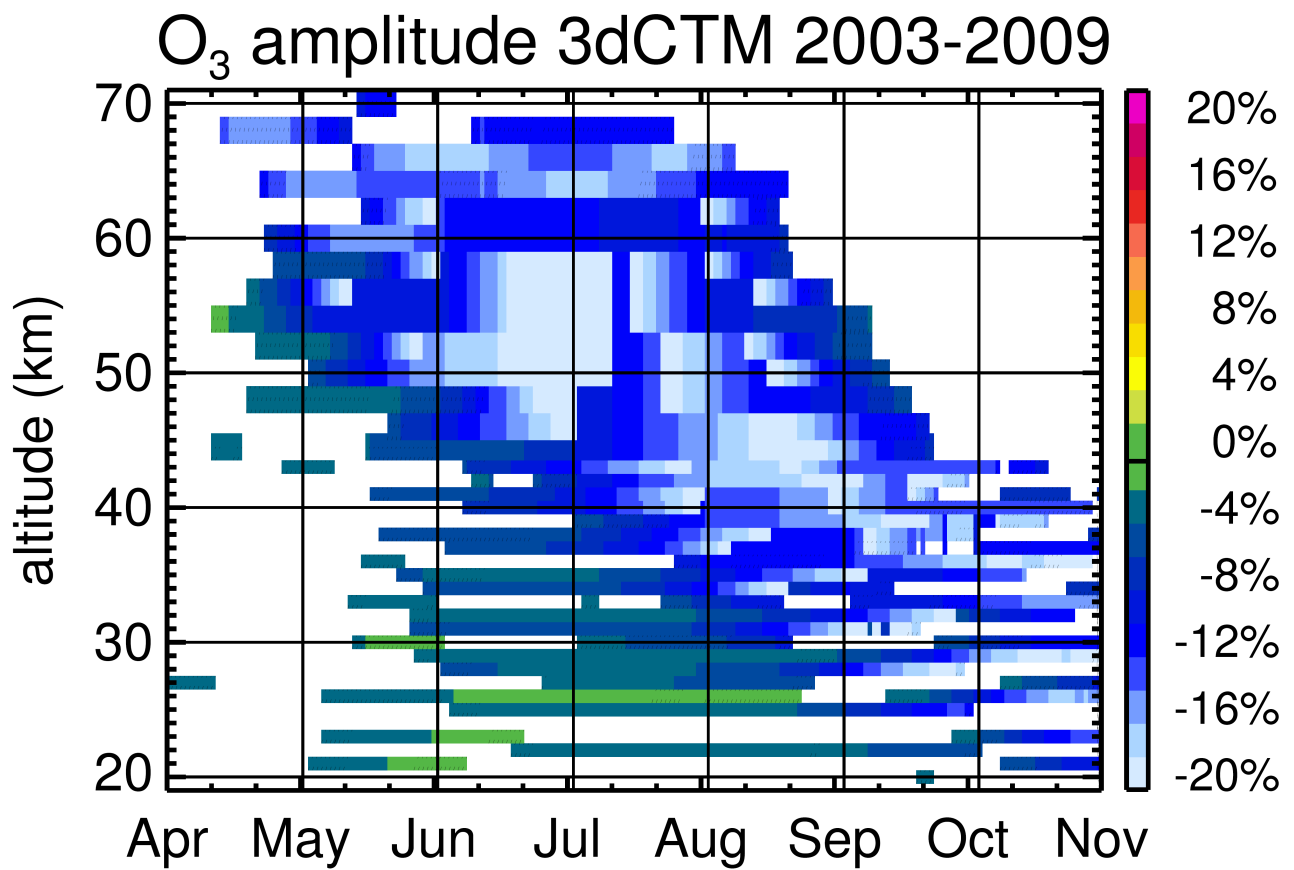


1
 2 Figure 5. Same as Figure 3 but only for Ap index (upper row) and ≥ 2 MeV electron flux (lower
 3 row) from 2005 – 2010.



1
2 Figure 6. Same as Figure 3, but only for the NO₂ amplitude associated to 1 April Ap index. The NO₂
3 was derived from MIPAS observations from 2005 – 2010.

4
5



1

- 2 Figure 7. O₃ amplitude (see Sect. 2.4 for definition), simulated by the 3dCTM from 2003 – 2009.
- 3 Shown are values above 95% significance level, according to a Student's t-test, and areas between
- 4 95% and 99% significance level are shaded.